The Astrophysical Journal, 572:753–761, 2002 June 20

ARE THE NARROW-LINE REGIONS IN ACTIVE GALAXIES DUSTY AND RADIATION PRESSURE DOMINATED?

Michael A. Dopita, Brent A. Groves, and Ralph S. Sutherland
Research School of Astronomy and Astrophysics, Institute of Advanced Studies, Australian National University, Cotter Road, Weston Creek, ACT 2611, Australia; Michael.Dopita@anu.edu.au, bgroves@mso.anu.edu.au, ralph@mso.anu.edu.au

Luc Binette
Instituto de Astronomia, Universidad Nacional Autonoma de Mexico, Apartado Postal 70-264, DF 04510, Mexico

and

Gerald Cecil
Department of Physics and Astronomy, University of North Carolina, Chapel Hill, NC 27599-3255
Received 2001 August 2; accepted 2002 February 25

ABSTRACT

The remarkable similarity between emission spectra of narrow-line regions (NLRs) in Seyfert galaxies has long presented a mystery. In photoionization models, this similarity implies that the ionization parameter is nearly always the same, about $U \sim 0.01$. Here we present dusty, radiation pressure–dominated photoionization models that can provide natural physical insight into this problem. In these models, dust and the radiation pressure acting upon it provide the controlling factor in moderating the density, excitation, and surface brightness of photoionized NLR structures. Additionally, photoelectric heating by the dust is important in determining the temperature structure of the models. These models can also explain the coexistence of the low-, intermediate-, and coronal ionization zones within a single self-consistent physical structure. The radiation pressure acting on dust may also be capable of driving the fast ($\sim$3000 km s^{-1}) outflows such as are seen in the *HST* observations of NGC 1068.

Subject headings: galaxies: active — galaxies: Seyfert — ISM: general — line: formation

1. INTRODUCTION

Optical spectroscopy of the ionized gas around galactic nuclei provides strong constraints on the excitation mechanisms. Line ratio diagrams of active galactic nuclei (AGNs), such as those of Veilleux & Osterbrock (1987), allow us to distinguish three major classes: nuclei excited by starbursts and the two types excited by a bona fide active nucleus—the Seyfert narrow-line regions (NLRs) and extended narrow-line regions (ENLRs), and the low-ionization nuclear emission-line regions (LINERs). As far as the Seyfert galaxies are concerned, the compilations of Veilleux & Osterbrock (1987), Veilleux (1991a, 1991b, 1991c), and Véron-Cetty & Véron (2000) show that the emission-line ratios are remarkably uniform within a given object and very similar (with typically less than 0.5 dex variation) from one object to another.

The standard paradigm proposes that the NLR and the ENLR are excited by photons originating at or near a compact nuclear source (see, e.g., Osterbrock 1989) having a smooth, featureless power-law or broken power-law EUV-ionizing spectrum. Within this model, the clustering of the observed line ratios within such a restricted domain of parameter space presents a problem, since in such models the excitation is in large measure controlled by the ionization parameter, U, and this is free to vary over a wide range. The implications of this is that there should exist photoionized regions with very high excitation corresponding to high U, but objects such as these are missing in the Veilleux & Osterbrock (1987) diagnostic diagrams. Instead, the constraints derived from the line ratio diagnostic diagrams imply that U has a similar value in all NLRs. Modelers have been therefore forced to make the arbitrary (and possibly unphysical) assumption that the gas density in the ionized clouds must fall exactly as the inverse square of the distance from the nucleus.

One rather successful variation on the photoionization models is to assume that the power-law EUV spectrum passes through a highly ionized screen of diffuse gas before being absorbed in the vicinity of dense (much higher pressure) clouds (Binette et al. 1996, 1997). Although such models produce generally good results when compared with observed ratios, these have the difficulty that the geometry of the ionized gas is ill-defined and necessarily becomes a new free parameter. These models can also be questioned on physical grounds, since the assumed pressure difference between the cloud and intercloud components is not explained.

Another variation is to consider the integrated emission from a whole family of photoionized clouds of different densities (Komossa & Schulz 1997; Ferguson et al. 1997). These models can be made to fit the observed spectra quite well, but the geometry of the clouds and their relative contributions to the emission remain free parameters and are poorly constrained.

In any of these photoionized models, the (often quite violent) internal dynamics of the ENLR are not addressed. These include clear evidence of nongravitational motion and evidence of outflow at velocities of up to (or even in excess of) 1000 km s^{-1} (e.g., Pedlar et al. 1989; Allen et al. 1999). Results such as these led Wilson & Willis (1980) to suggest that the nucleus ejects radio components that interact with ambient gas and replenish the high kinetic energy and ionization of the NLR. This led to the development of photoionization by fast radiative shocks, which generate a strong internal photoionizing radiation field (Dopita &

Sutherland 1995, 1996). This model is successful in reproducing the strong lines observed in many AGNs (see review by Dopita 2000). In addition, it can explain other features that simple photoionization models fail to address. For example, where the NLRs are spatially resolved, strong correlations are often found between radio power and either line luminosity (de Bruyn & Wilson 1978) or line width (Wilson & Willis 1980). Such correlations not only exist for Seyfert galaxies, but they also persist up to much more luminous classes of radio galaxies. However, the fast-shock model has its limitations. It has difficulty reproducing the very strong coronal lines of [Fe VII], [Fe X], [S VIII], [S XII], [Si VI], or [Si VII] (Wilson & Raymond 1999), which imply photoionization with very high local ionization parameters. These models also cannot reproduce the large outflow velocities inferred in the [O III] line in some objects such as NGC 1068 (e.g., Kraemer & Crenshaw 2000; Cecil et al. 2002). In shock models, most of the [O III] emission is expected to be generated in the photoionized precursor of the shock, which theoretically should be the undisturbed gas in the galaxy. Furthermore, the NLR lines of (probably) the majority of Seyfert galaxies are quite narrow and consistent with line broadening due to galactic rotation rather than being produced in shocked outflows.

In this paper we argue that some of these properties can be explained in terms of radiation pressure–dominated dusty photoablating clouds. In the past, dust has been considered in photoionization models both through its contribution via photoelectric heating (e.g., Bottorff et al. 1998) and as a shielding component, thanks to its large opacity in the FUV. However, the effects of dust photoelectric heating and of the radiation pressure on dust on both the ionization and hydrostatic structure of the NLR clouds has not been examined in a systematic fashion before. In § 3 we detail these effects and show how these provide a natural explanation as to why the inferred NLR ionization parameter seems to be confined to the range $-2.5 < \log U < -2$. In § 3 we describe the basics of our dusty, radiation pressure–dominated models. These are compared with other types of photoionization models, allowing us to separately understand the effects of photoelectric heating and of radiation pressure on the emergent spectrum. The predictions of all these models are compared with observations of NLR of Seyfert galaxies on some key emission-line diagnostic diagrams. The concluding remarks are given in §4. In future papers we will investigate further the effects of different parameters on our radiation pressure–dominated photoionization models and present a full hydrodynamic model exploring such structures.

2. A NEW PARADIGM: DUSTY, RADIATION PRESSURE–DOMINATED PHOTOIONIZATION

The effects of radiation pressure from line absorption have previously been considered in photoionization models of the emission-line regions of AGNs (Elitzur & Ferland 1986). This is important in determining the internal density structure at large ionization parameters. The effect of dust within the ENLR has also been considered previously (Netzer & Laor 1993). However, the radiation pressure exerted by the ionizing source acting upon dust within the photoionized gas has usually not been accounted for by the standard photoionization models, with a few notable exceptions (e.g., Baldwin et al. 1991, who examined the Orion Nebula, and Pier & Volt 1995, who considered the inner edge of dusty torii in AGNs and the generation of coronal emission lines). The standard photoionization modeling assumes an isochoric (or constant density) structure within the ionized slab instead of an isobaric (constant pressure) structure. Dust is important not only because of the radiation pressure acting upon it, but also because of the photoelectric heating that it produces in the photoionized plasma and in the way it competes with the gas in absorbing the ionizing photons.

However, all of this critically depends on whether dust can survive either the strong EUV radiation field or the relatively energetic conditions characterizing the photoionized region. In the ionized plasma of the ENLR, grains are electrically charged, locking the motion of the dust to that of the ionized gas. Both the ionized gas and the dust are likely to be streaming at roughly sonic velocities from ionization fronts located around photoevaporating dense clouds located in the "ionization cones" of the AGNs. The problem of dust survival is therefore reduced to the question of whether it can survive for a time equal to its passage through the high-emissivity region near the cloud surface, as discussed in § 3. Our detailed photoionization models show that the average gas temperature is $\sim 10^4$ K, at which point the thermal sputtering of grains is negligible and incapable of destroying the grains in so short a timescale. This is in contrast with the case of radiative shocks in which gas temperatures reach $\sim 10^5$–10^6 K and grain destruction by sputtering occurs on very short timescales (Tielens et al. 1994). Similarly, our models show that grain temperatures are too low for thermal evaporation of grains by quantum heating, provided that the dust grains are large enough ($\gtrsim 3$ nm). A third potential dust destruction mechanism is that of Coulomb explosion, in which the grain charging becomes large enough that the Coulomb repulsion between the atoms composing the grain exceeds the atomic bond strength. According to our models, this condition is met for grains smaller than about 10 nm when the ionization parameter is of order unity. In the models described here, we have simply set the minimum grain radius equal to 10 nm to allow for the destruction of the smaller grains. We will return to the detailed physics of grain destruction processes in these environments in a future paper.

In NLR regions observed by Oliva et al. (1994), Moorwood et al. (1996), and Kraemer & Crenshaw (2000), the coronal lines appear remarkably strong, as compared to Hβ. The existence of such coronal gas requires that both the ionization parameter and the radiation pressure are very large (Binette et al. 1997). Elements such as Fe and Si are normally largely sequestered in the grains. The strength of the coronal lines of these elements requires that in the coronal gas, at least, the dust has been largely destroyed. Our model, as depicted in Figure 1, is therefore one of a dusty, radiation pressure–dominated region surrounding a photoevaporating molecular cloud, which in turn is surrounded by a coronal halo within which the dust has been largely destroyed. In this paper we will consider only the emission spectrum generated by the dusty dense inner region near the stagnation point in the flow around the cloud. This will be the highest emissivity region in the flow, and it will be the region in which the radiation pressure gradient is matched by the gas pressure gradient, allowing us to construct static rather than dynamic photoionization models.

Consider Ξ_0, the ratio of the available pressure of ionizing radiation, Φ, to the gas pressure at the irradiated photoion-

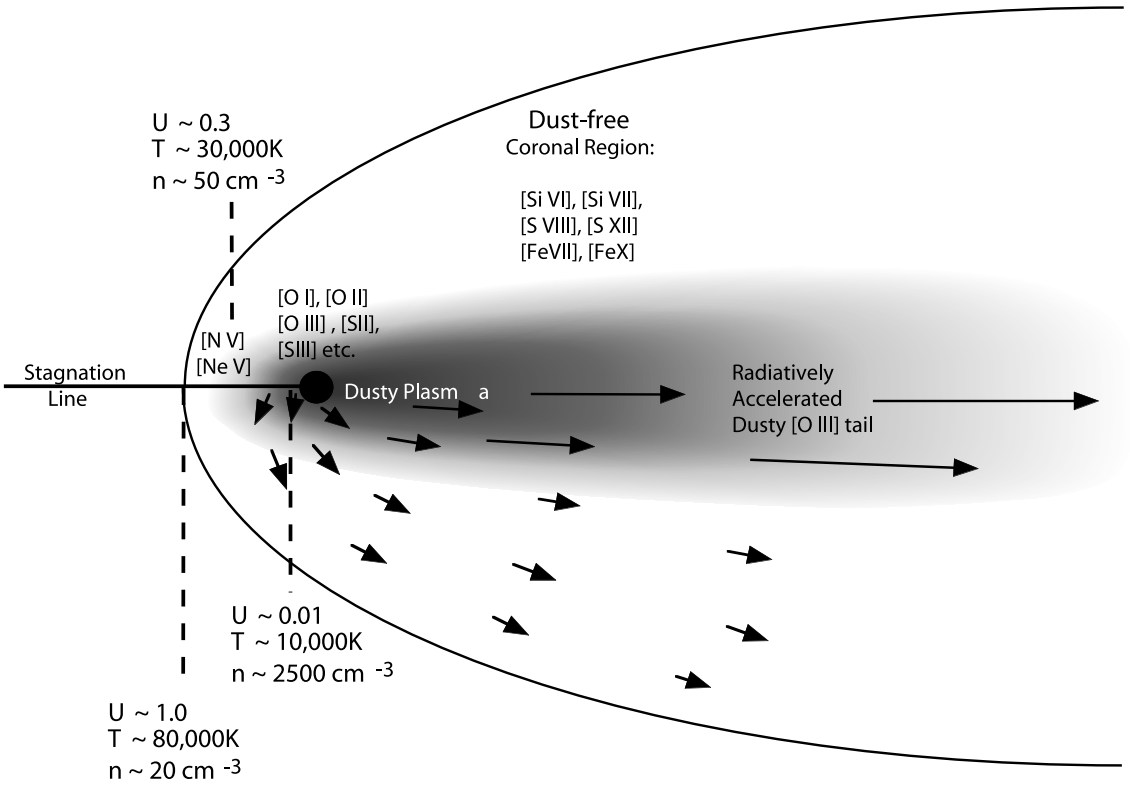

FIG. 1.—Depiction of our theoretical model showing the photoevaporating, dusty molecular cloud (*filled circle*) at the center surrounded by the dusty, photoevaporated plasma, from which both the low- (close to the cloud) and intermediate-ionization (close to the coronal region) lines are emitted. This plasma is itself surrounded by the dust-free coronal region. The stagnation line indicates the region modeled by this paper. Each region (excluding the molecular cloud) is marked with some of the strong lines emitted from this part of the structure. The parameters marked by the dashed lines indicate typical values for each region for a NLR cloud found in NGC 1068.

ized surface of a photoevaporating cloud,[1]

$$\Xi_0 = \frac{P_{\rm rad}}{P^0_{\rm gas}} \simeq \frac{\Phi_0/c}{2.3nkT_e} \approx U_0 \frac{\langle \varepsilon_{\rm EUV} \rangle}{2.3kT_e} , \qquad (1)$$

where k is Boltzmann's constant, c is the speed of light, and n and T_e are the hydrogen density and the electron temperature at the irradiated cloud surface (indicated by a subscript zero elsewhere). We define $S_* = \Phi_0/\langle \varepsilon_{\rm EUV} \rangle = \int [\varphi_0(\nu)/h\nu] d\nu$ to be the ionizing photon flux ($\rm cm^{-2}\ s^{-1}$) impinging at the surface such that $U_0 = S_*/nc$ is the canonical ionization parameter; $\langle \varepsilon_{\rm EUV} \rangle$ ($= \langle h\nu_{\rm EUV} \rangle$) is the local average EUV photon energy.

In hydrostatic equilibrium, the gas pressure gradient must match the local radiative volume force exerted by photon absorption, and this force can be separated into its two components: the force acting on the gas through photoionization, and the component due to dust absorption,

$$F_{\rm rad}(x) = \sum_{m=1} \sum_{i=0} n_i(X^{+i}_m) \int_{\nu^i_m}^{\infty} \frac{\varphi(\nu)}{c} a_\nu(X^{+i}_m) d\nu + n_{\rm H} \int_{\nu^k_m}^{\infty} \{\kappa_{\rm abs}(\nu) + \kappa_{\rm sca}(\nu)[1 - g(\nu)]\} \frac{\varphi(\nu)}{c} d\nu , \qquad (2)$$

where $\varphi(\nu)$ is the local radiation flux at frequency ν, $n_i(X^{+i}_m)$ is the number density of ion $+i$ of atomic species m, and $a_\nu(X^{+i}_m)$ is the corresponding photoionization cross section with threshold ν^i_m. In the dust absorption term, $\kappa_{\rm abs}(\nu)$ and $\kappa_{\rm sca}(\nu)$ is the dust absorption cross section and scattering cross section, respectively, normalized to the hydrogen density, and $g(\nu) = \langle \cos \theta_\nu \rangle$ is the mean scattering angle of the dust grains at this frequency. The boundary condition is given by P_0, the pressure at the irradiated face.

We can readily estimate a critical value of U_0 above which dust absorption dominates over the photoelectric absorption. For an equilibrium photoionized plasma, the absorption of ionizing photons in a slab is simply equal to the local recombination rate in the plasma,

$$\frac{dS_*}{dx} = -\alpha_B n^2 ,$$

where α_B is the recombination rate to excited states of hydrogen. The absorption of ionizing photons by dust is given by

$$\frac{dS_*}{dx} = -\kappa n S_* ,$$

where κ is the effective dust opacity of order $\sim 10^{-21}$ $\rm cm^2$ (H atom)$^{-1}$. Dust absorption becomes relatively more important as the strength of the ionizing field increases, and dust becomes the dominant opacity in the plasma when

$$U_0 > \frac{\alpha_B}{c\kappa} . \qquad (3)$$

[1] This definition implies a factor of 2.3 less value than that of Krolik, McKee, & Tarter (1981).

For a typical value of $\alpha_B = 2 \times 10^{-13}$ cm^3 s^{-1}, the critical ionization parameter is $\sim$0.007.

This value is closely related to that at which radiation pressure starts to dominate either the gas pressure or the dynamical acceleration of the plasma. If $\langle \varepsilon_{\rm EUV} \rangle$ is the mean energy of the ionizing photons absorbed by gas, and $\langle \varepsilon_{\rm FUV} \rangle$ is the mean energy of the ionizing absorbed by dust, then equation (2) can be approximated by

$$F_{\rm rad}(x) = \frac{1}{c}\,\alpha_B n^2 \langle \varepsilon_{\rm EUV} \rangle + \frac{1}{c}\,S_* \langle \varepsilon_{\rm FUV} \rangle \kappa n = \frac{n^2 \langle \varepsilon_{\rm EUV} \rangle}{c} \left(\alpha_B + \frac{\xi}{\psi}\,U_0 \kappa c \right), \quad (4)$$

where $\langle \varepsilon_{\rm EUV} \rangle / \langle \varepsilon_{\rm FUV} \rangle = \psi$ and the effective ionization parameter for the dust-absorbed photons is $U_{\rm FUV} = \xi U$. Generally speaking, both ξ and ψ will be greater than unity. Clearly, dust becomes the dominant term in this equation when

$$U_0 > \frac{\psi \alpha_B}{\xi c \kappa}\,. \quad (5)$$

This expression is the same as equation (3) except for the ratio ψ/ξ, which is of order unity. In the typical ionization field expected around an AGN, $\varphi_0(\nu) \propto \nu^{-1.4}$, and with a "standard" dust model with solar abundances, a Mathis, Rumpl, & Nordsieck (MRN) size distribution (1977) $n(a) \propto a^{-3.5}$, and a lower size cutoff of 10 nm, we estimate that this condition gives a critical ionization parameter $U_0 \sim 0.01$.

If the ionization parameter into a static plane-parallel slab of ionized gas is increased above this critical value, then the radiation pressure gradient imposed as the EUV radiation field is absorbed through the ionized slab and will induce a corresponding local gas pressure gradient. Thus, if the initial (outer layer) pressure of the ionized gas is P_0 and the radiation pressure in the EUV field is $P_{\rm rad}$, then the gas pressure close to the ionization front is $P_0 + P_{\rm rad}$. Thus, at high ionization parameters, the pressure in the ionized gas close to the ionization front is *determined* by the externally imposed ionization parameter, U_0, and the *local* ionization parameter becomes independent of the initial ionization parameter. In this way, the emission-line spectrum in the low- and intermediate-ionization species will become effectively independent of the external ionization parameter. This is the core of our explanation of why the emission-line spectra of NLR are so similar one to another.

While U_0 defines the ionization parameter at the face of the cloud, one can define a *mean* ionization parameter $\bar{U} = S_*/\bar{n}c = U_0 n_0/\bar{n}$, where $\bar{n}$ is simply the mean density, that is, an emissivity-averaged density using a weight $\propto n_e^2$. Binette et al. (1997) showed that $\bar{U}$ tends asymptotically toward a constant value in the limit of high U_0.

3. RESULTS OF MODELS

We have constructed static, plane-parallel, radiation pressure–dominated, dusty photoionization models using the code MAPPINGS III, which includes the implementation of equation (2) to evaluate the local radiation pressure gradient and hence the local density gradient. MAPPINGS III treats several of the properties of dust, such as photoelectric heating, as described previously by Dopita & Sutherland (2000). The dust model includes both silicaceous and carbonaceous grains with an MRN grain size distribution and uses the absorption and scattering data of Laor & Draine (1993, using the more recent smoothed UV data for silicates).[2] Here we have chosen the simplest "standard" values for the input parameters. For example, the models all used the Anders & Grevesse (1989) solar abundance set, with the depletion factors for each element given in Table 1. The input ionizing spectrum for the following models was a standard power-law continuum with $\varphi_0(\nu) \propto \nu^{-1.4}$. The effect of varying these and other input parameters will be investigated in a future paper (B. A. Groves et al. 2001, in preparation).

TABLE 1
SOLAR METALLICITY ($Z_\odot$) AND DEPLETION FACTORS (D) ADOPTED FOR EACH ELEMENT

Element	$\log(Z_\odot)$	$\log(D)$
H	0.00	0.00
He	−1.01	0.00
C	−3.44	−0.30
N	−3.95	−0.22
O	−3.07	−0.22
Ne	−3.91	0.00
Mg	−4.42	−0.70
Si	−4.45	−1.00
S	−4.79	0.00
Ar	−5.44	0.00
Ca	−5.64	−2.52
Fe	−4.33	−2.00

To facilitate comparison and to separate the effects of internal density structure, radiation pressure, and photoelectric heating by the grains, we have run four families of models with increasing ionization parameter U_0 (defined at the outer boundary of the ionized slab). We present them in order of increasing physical sophistication (and reality):

1. Isochoric (constant density) dust-free models with heavy-element abundances in the gas phase that match those of the models that include dust.
2. Isobaric dust-free models. Again, these have gas-phase heavy-element abundances that match the models with dust. These models are isobaric in the sense that the product nT is kept constant, but the radiation pressure is not explicitly included.
3. Isochoric dusty models.
4. Isobaric dusty models without radiation pressure. These provide a dusty comparison to the complete model, which shows the difference that radiation pressure makes.
5. Complete isobaric dusty models, which include the effect of radiation pressure on the density structure of the ionized gas.

To avoid differential effects caused by different electron density in the low-excitation cases, in all cases the initial density was adjusted so that the density of the region emitting in the [S II] lines was maintained constant at about 550 cm^{-3} to within 10%. This density was chosen to be typical of

[2] Available at http://www.astro.princeton.edu/~draine/dust/dust.diel.html.

the electron densities inferred from the [S II] $\lambda6717/\lambda6731$ ratio in the NLRs of Seyfert galaxies. The models were terminated at a point where the gas temperature dropped rapidly to below 5000 K and the emission in the optical forbidden lines is quenched.

Generally, in the literature we encounter only the first or the third of these sets of models. The profound difference in the internal structure of the isobaric dusty models that include radiation pressure compared with a "standard" isochoric model is emphasized in Figure 2, which shows the internal density and temperature structure produced in the dusty, radiation pressure–dominated slab model with ionization parameter of $U_0 = 0.5$. In this model, the radiation pressure in the EUV radiation field is roughly 30 times the initial gas pressure. At the "front" surface of the cloud, the opacity of the cloud is entirely dominated by dust, and the photoelectric heating by dust is very large. As a consequence, the electron temperature in this zone is very high, of order 25,000 K. The electron temperature decreases strongly throughout the model toward the ionization front, and this steepens the density gradient in the model.

This strong density gradient, which is set up between the high-ionization and low-ionization regions, can provide a physical explanation of the pressure difference between these regions, which was required in the A/M_I models of Binette et al. (1996). As expected, the pressure in the low-ionization region scales with the radiation pressure at high U_0. Thus, the local ionization parameter characterizing the low- and intermediate-ionization region of the model becomes independent of U_0.

The emission-line ratios produced by the various classes of models can be quite different one from another. We have chosen to display here only those that provide a good separation between the different classes of models and thus have a diagnostic utility. Any of the line emission ratios used by Veilleux & Osterbrock (1987) will give such a separation.

In Figure 3 we plot one of these diagnostic diagrams, the [S II] $\lambda6717 + \lambda6731/\mathrm{H}\alpha$ ratio versus the [O III] $\lambda5007/\mathrm{H}\beta$ ratio. The observational points are from Allen et al. (1999). For the dust-free case, neither the isochoric nor the isobaric sequence can reproduce the observed data, although the fit would be improved with a flatter spectral index. The closest fit is found in the region $\log U_0 \sim -2.8$. As has been shown by many other authors, only a very restricted range of ionization parameters provides a reasonable fit.

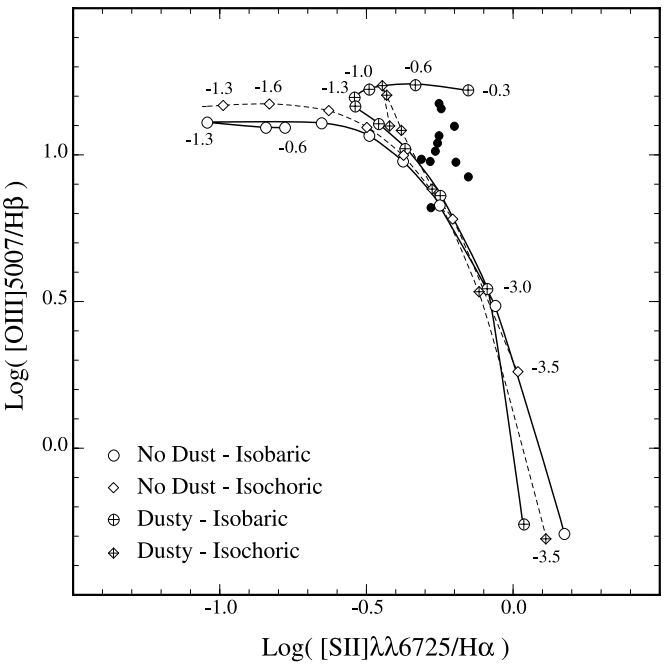

FIG. 3.—Line diagnostic diagram of [O III] $\lambda5007/\mathrm{H}\beta$ vs. [S II] $\lambda\lambda6717,\ 6731/\mathrm{H}\alpha$, showing the output from four families of models. These are split into two dust-free models (*open markers*) and two dusty models (*crossed markers*), with an isochoric model (*dashed lines*) and an isobaric model (*solid lines*) in each case. The isobaric, dusty model also includes the effect of radiation pressure. Along each model, line marks indicating log U_0 are shown. The solid circles are observations from Allen et al. (1999). Note that the dust-free cases do not match the observations, whereas both dusty models provide reasonable solutions.

For the dusty models, both the isochoric and isobaric sequences approach the region of the observed NLR at high ionization parameters. The dusty, radiation pressure-affected isobaric model shows very slow variation in the line ratios with U at high ionization parameters, and these line ratios are in the region of interest. The dusty, isochoric models actually begin to head away from the observations as we increase in ionization parameter.

Figure 4 is a close-up of the region of interest, showing only isobaric models. In addition to the two isobaric models described above, a dusty, isobaric model without radiation pressure is included for comparison. This figure illustrates the self-regulating effect of the radiation pressure in producing nearly constant line ratios for $U_0 > 10^{-2}$. While the radiation pressure-free case does reproduce the observed data quite well, it does so only for a small range of ionization parameters, $-2.3 < \log U_0 < -1.3$. By $\log U_0 \sim -1.0$, the model has left the region in which the observations lie. The complete dusty models, which include the effects of radiation pressure, not only lie in the region of the observed data but also display line ratios that stagnate with respect to changes in U over a broad range of values. The implication of this is that, provided $U_0 \gg 10^{-2}$, a cloud of given density could be moved radially by a large amount without producing any appreciable change in its excitation state. Such behavior is frequently seen and is interpreted in the "classical" photoionization models as indicating a constant ionization parameter.

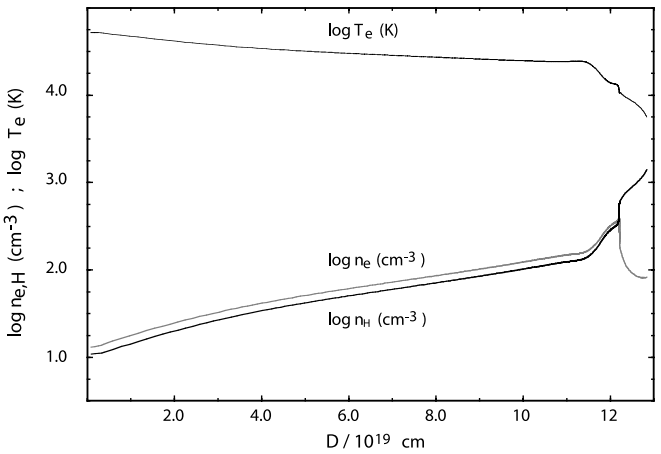

FIG. 2.—Temperature and density structure in a radiation pressure–dominated, dusty model with $U_0 = 0.5$.

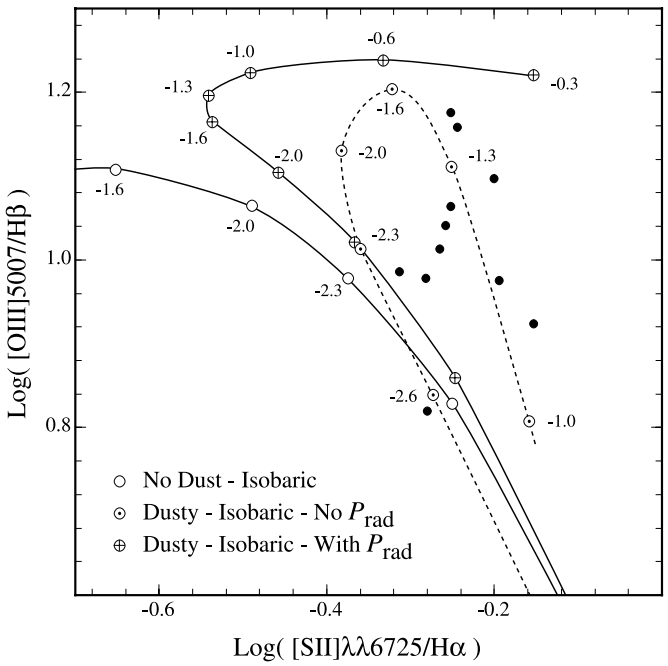

FIG. 4.—Close-up of the region of interest in Fig. 3, showing only the isobaric models. As well as the dust-free isobaric model (*open circles*) and the dusty, radiation pressure-affected model (*crossed circles*) from Fig. 3, a dusty model without the effects of radiation pressure is included (*dashed line with dotted circles*). Note the model without P_{rad} does match the observations well, but the line ratios do not stagnate with changes in U like the complete dusty model.

The conclusions derived from Figures 3 and 4 are reinforced when we replace the [O III] line by the higher excitation [Ne V] line. This is shown in Figure 5. Now the range of acceptable models is appreciably reduced. From inspection of both Figures 3 and 5, we see that the dusty models that include radiation pressure provide acceptable solutions in the range $-1.6 < \log U_0 < 0$. The acceptable range of solutions for the dusty isochoric models is much more restricted, $-2.0 < \log U_0 < -1.2$, and there are no truly acceptable solutions for *any* dust-free model. This illustrates a major advantage of the radiation pressure–dominated model in that it encompasses a wider range of ionization species than any simple isochoric or isobaric model. The reason for this is that as density increases inward, one is effectively spanning a very wide range in the local ionization parameter. Furthermore, the extra heating provided by dust photoheating scales with U_0 and the higher electron temperatures enhances the intensities of the high-ionization species in a way that the dust-free models cannot account for. This effect is further enhanced by dust absorption that strongly reduces the luminosity of the hydrogen recombination lines in the high-ionization zone. At the same time, it enhances the He II $\lambda 4686/\mathrm{H}\beta$ ratio to values as high as 0.5–0.6, which is in better agreement with observation and similar to the values obtained in the matter-bounded models of Binette et al. (1996).

If we look only at line ratios that are sensitive to the excitation, then dust-free models might seem to provide an acceptable fit. An example is shown in Figure 6, which plots the [O III]/[O I] line ratio against the [Ne V]/[Ne III] ratio. Here, similar values of the ionization parameter produce very similar values of the [Ne V]/[Ne III] ratio, while the [O III]/[O I] line ratio is more strongly affected by the temperature in the [O I]-emitting zone. Note that again the dusty models that include radiation pressure provide acceptable solutions in the range $-1.6 < \log U_0 < 0$.

The effect of photoelectric heating is best investigated in terms of the electron temperature in the [O III]-emitting

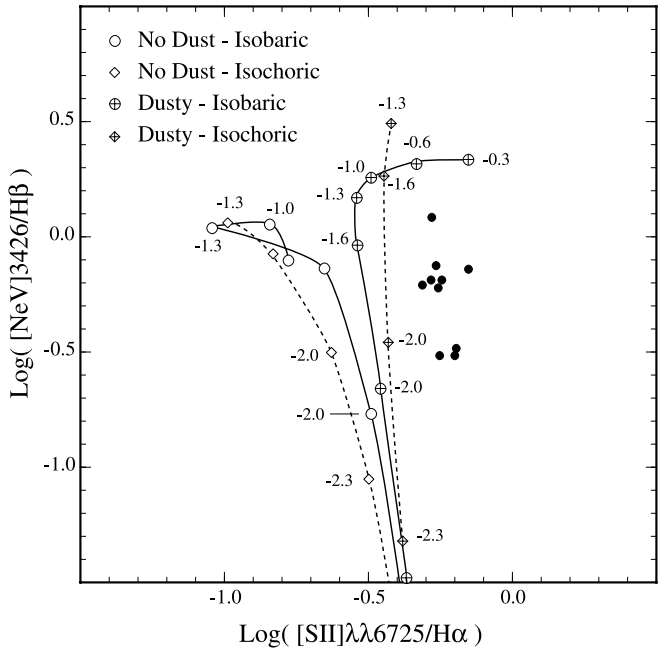

FIG. 5.—Line diagnostic diagram of [Ne V] $\lambda 3426/\mathrm{H}\beta$ vs. [S II] $\lambda\lambda 6717,\ 6731/\mathrm{H}\alpha$ with the same symbols as Fig. 3. Note that, in consideration with Fig. 3, only the dusty models provide reasonable solutions to the isochoric case with $-2.0 < \log U_0 < -1.2$ and the isobaric case with $-1.6 < \log U_0 < 0$.

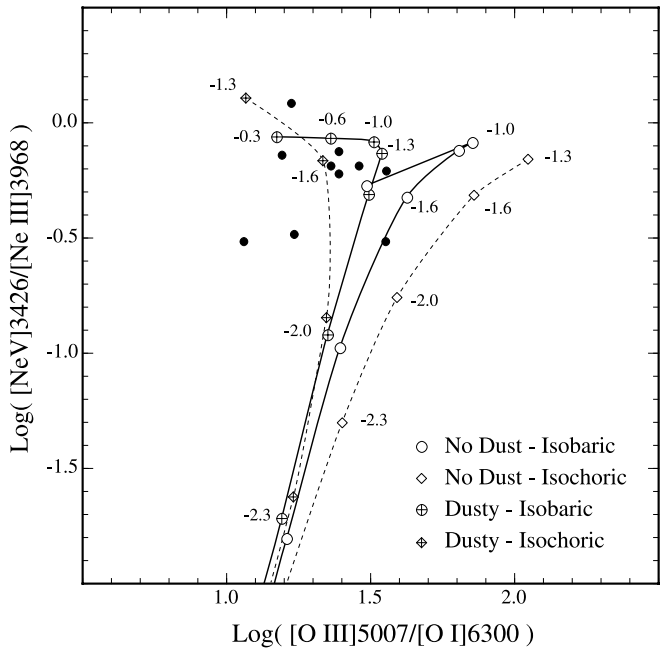

FIG. 6.—Line diagnostic diagram of [Ne V] $\lambda 3426/[\mathrm{Ne\ III}]\ \lambda 3968$ vs. [O III] $\lambda 5007/[\mathrm{O\ I}]\ \lambda 6300$, with the same symbols as Fig. 3. Note that these line ratios are sensitive to excitation, and with inspection of this and of Figs. 4 and 5, it can be seen that again the isobaric dusty model provides a reasonable solution between $-1.6 < \log U_0 < 0$.

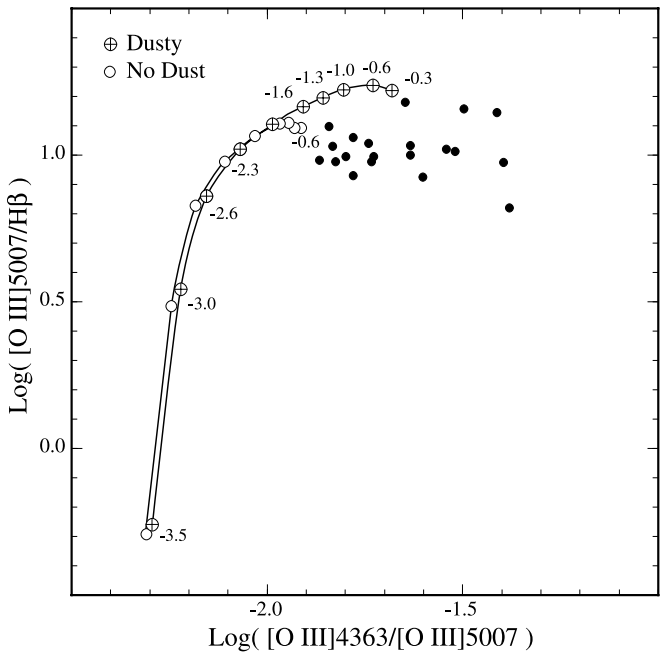

FIG. 7.—Line diagnostic diagram of [O III] λ5007/Hβ vs. [O III] λ4363/λ5007 with two cases: a dust-free isobaric model (*empty circles*) and a dusty, isobaric model with radiation pressure model (*crossed circles*). The marks on the model lines indicate log U_0. The solid circles are observations drawn from both Allen et al. (1999) and Tadhunter et al. (1989). Note that with the consideration of Figs. 3–7 that the isobaric, dusty, radiation pressure-affected models provide the most acceptable solutions, with $-1.6 < \log U_0 < 0$.

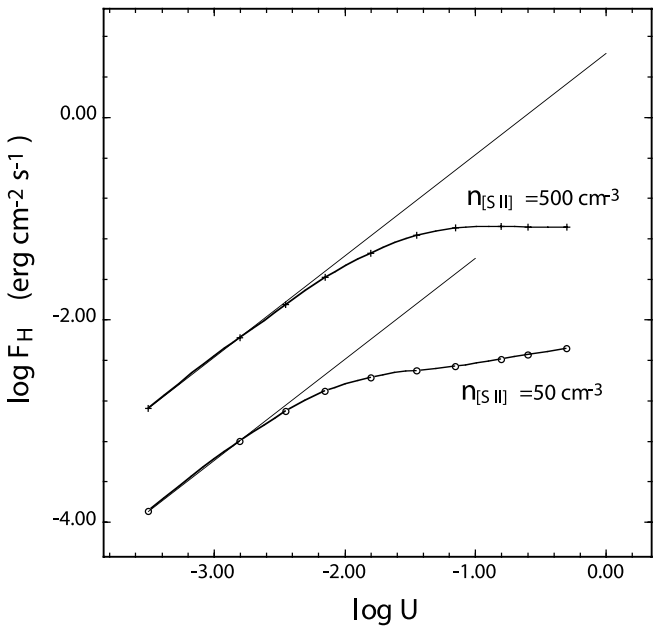

FIG. 8.—Hβ flux vs. ionization parameter, showing two groups of models. The two groups shown differ in density, with the crosses indicating a density at the back of the cloud of $\sim$550 cm^{-3} and the circles indicating $\sim$55 cm^{-3} (as labeled). Within each group, the thin lines show a "standard" (isochoric) model without dust, and the thick lines show the result from our radiation pressure–dominated, dusty model, showing the limiting of the Hβ flux.

region. This is shown in Figure 7, which plots the temperature-sensitive [O III] λ4363/λ5007 ratio against [O III] λ5007/Hβ. For clarity, we have omitted the isochoric models, since these largely overlap with the isobaric cases. The observed points are drawn from both Allen et al. (1999) and Tadhunter, Robinson, & Morganti (1989). The dust-free models are clearly much cooler than the dusty models and fail to reproduce the observed [O III] temperatures for any ionization parameter. This is the famous "temperature problem" of NLR, which was discussed in detail by Tadhunter et al. (1989). Photoelectric heating by dust, proposed as the solution to a similar problem occurring in planetary nebulae by Dopita & Sutherland (2000), seems to provide enough additional heating in NLR to bring the predicted electron temperatures into the observed range. Once again, for dusty isobaric radiation pressure–dominated models, acceptable models for the [O III] λ4363/λ5007 ratio lie in the range $-1.6 < \log U_0 < 0$.

A final major effect of the addition of dust in these models is to limit the Hβ surface brightness as a consequence of the absorption of ionizing photons by dust. Since dust absorption strongly dominates over the gas absorption in the regime of high ionization parameter, this limits the ionized column (Strömgren column) to a maximum value. For a fixed density or pressure in the region emitting the [S II] lines, the surface brightness of the ionized zone in Hβ saturates at a maximal value at high U_0. By contrast, at low U_0, dust absorption is negligible compared with gas absorption, and the Hβ flux scales with the ionization parameter. This behavior is shown in Figure 8.

If the [S II] density is lowered, then at a given U_0 the Hβ flux simply scales with the density in the low-U_0 regime. However, since the dust and the gas absorption terms have a different density dependence, at a given U_0 in the high-U_0 regime, a lowering of the density in the [S II] zone leads to a greater fraction of the incident radiation field being absorbed by dust. The result of this is that the saturation value of the Hβ surface brightness is reduced by a greater factor than simply the ratio of the densities. The roll-off between the low-U_0 and high-U_0 regimes must therefore occur at a slightly lower value of U_0 than in the high-density case.

The plane-parallel models presented here strictly apply only along the (stagnation) line, which lies directly toward the ionizing source on the front face of a photoevaporating cloud. Toward the sides of the cloud, lateral motions will be developed in the ionized plasma by the transverse gas pressure gradient. Around the cloud edges, the radiation pressure force acts radially outward from the central engine. According to equation (2), this drives an accelerating flow radially away from the central AGN. Such a radiatively driven outflow was considered by Binette (1998) in the context of the coronal gas. In the case of NGC 1068, new *HST* STIS data presented by Cecil et al. (2002) shows [O III] tails of clouds about 100 pc away from the nucleus being accelerated up to 2000 km s^{-1} or greater over a distance of about 0$''$.15 (10 pc). This corresponds to an acceleration of order 6×10^{-4} cm s^{-2}. Let us now examine whether this acceleration could be due to radiation pressure.

According to the observations of Kraemer & Crenshaw (2000), the density given by the [S II] lines in NGC 1068 is about 2500 cm^{-3}. In the high ionization parameter models, this density is determined entirely by the radiative pressure, and such a pressure is obtained from a central source giving a surface luminosity of $\sim$1500 ergs cm^2 s^{-1} at the outer

boundary of the photoablating cloud. This figure is in excellent agreement with that inferred from the bolometric FIR luminosity (Dopita et al. 1998), $\sim 1.5 \times 10^{11}\ L_{\odot}$. This gives a flux at a distance of 70 pc from the nucleus (typical for these clouds) of about 1700 ergs cm^2 s^{-1}.

If these radiative forces go into accelerating the gas in the ionized tails of the NGC 1068 clouds, then from equation (4) we would require a flux of order 1.5×10^4 ergs cm^{-2} s^{-1} to provide the observed acceleration. The inferred flux is a factor of 10 lower than this, and this would produce a final outflow velocity of order 700 km s^{-1}. The only way around this problem would be to increase the force per unit mass of gas by increasing dust opacity. This could be done through grain shattering, which, according to Jones, Tielens, & Hollenbach (1996), will occur whenever grain-grain collision velocities are greater than the sound speed in the grain material, about 2 km s^{-1}. This could be achieved with either subsonic turbulence in the gas or subsonic radiatively driven grain drift velocities.

A potential mechanism for grain shattering is as follows: Close to the ionization front, and within it, the net grain charge is negative, being dominated by collisions. When the grains are charged, their motion is strongly coupled to the gas via Coulomb interactions. As the grains are advected with the gas flow from the ionization front, the local radiation field becomes stronger, and the charge on the grains becomes smaller as photoelectric charging becomes more important. Eventually, the net charge on an individual grain becomes zero as the collisional and photoelectric charging exactly balance. At this point, the grain can decouple from the gas flow, and radiative pressure forces push it back toward the ionization front. The terminal drift velocity that the grain can reach is determined by the gas density, ρ, and the radiation field intensity, F, $v_{\rm drift} = (F/c\rho)^{1/2}$. For the parameters computed for NGC 1068, this could amount to $\sim$200 km s^{-1}. However, long before this velocity is reached, the grain will become charged once more, and the grain motion is again locked to the gas motion. Thus, when their charge becomes zero, the grains will tend to oscillate about the position where this happens until another (charged) grain strikes and shatters them. The shattered fragments have their equilibrium point farther out in the ionized flow, and of course they are much more vulnerable to the other grain destruction mechanisms we have mentioned. In our models for NGC 1068, grains are completely shattered in the region that produces [Ne V] and [Fe VII].

The idea that the ionized tails of the cloudlets in NGC 1068 are driven by radiation pressure acting on the shattered dust seems a reasonable one, but it is clear that the full solution to this problem will require a hydrodynamic model that explicitly includes the grain physics and destruction processes. We intend to present such a model in a future paper.

If dust is indeed destroyed at some point in the outflow, then the gas will continue to flow outward from the cloud, but radiation pressure effects become relatively ineffective in determining the dynamics. In this case, the cloud will become surrounded by a highly ionized coronal region with an equilibrium electron temperature of order 8×10^4 K. On the basis of continuity of pressure, we estimate that in the case of NGC 1068, the density of this region is 10–20 cm^{-3} and therefore that the effective ionization parameter is of order unity or somewhat greater. This would be sufficient to explain the extreme degree of ionization observed in this coronal region (Kraemer & Crenshaw 2000).

Finally, let us examine whether the hypothesis that dust can be accelerated in the cometary tail of the cloud is also consistent with the hypothesis that dust can also be destroyed in entering the coronal region. From the acceleration in the tail (6×10^{-4} cm s^{-2}) and the length of the tail (10 pc), we can estimate the transit time of material through the tail, 10^4 yr. Along the stagnation line in the direction of the source, material flows off the cloud at about the sound speed, 20 km s^{-1}. However, the photoionization model for NGC 1068 shows that the thickness of the ionized zone is about 10^{18} cm. Therefore, the dusty plasma flows through this region in about 1.6×10^4 yr. These timescales are quite comparable, which strongly suggests that the length of the [O III] tails and the production of the coronal region in NGC 1068 are both moderated by the dust destruction, occurring on a timescale of order 10^4 yr.

4. CONCLUSIONS

In this paper we propose that the NLR and ENLR of Seyfert galaxies can be self-consistently modeled by radiation pressure–dominated dusty photoionized regions surrounding photoablating dense clouds. By using the code MAPPINGS III, we have shown that these display a strong density gradient increasing toward the ionization front, are characterized by strong photoelectric heating by the dust and are regions in which the dominant absorption of the ionizing continuum is due to the dust. In these models, the gas pressure close to the ionization front is determined by the radiation field. The models provide the following:

1. A line spectrum consistent with the observations and that remains approximately invariant against changes in U_0 that span a range larger than 2 orders of magnitude.
2. A higher electron temperature than can be achieved in standard photoionization models and that could help explain the long-standing "temperature problem" of NLR and ENLR.
3. An Hβ surface brightness that reaches a maximum value at high values of the initial ionization parameter U_0.

In addition, they may also offer an explanation for

1. the coexistence of the low-ionization zones with an extremely high ionization parameter coronal region and
2. strong radial radiative acceleration of dusty gas that may explain the broad and blueshifted [O III] profiles seen in many Seyfert galaxies.

We will systematically explore the properties of such models in future papers.

The work of L. B. was supported by the CONACyT grant 32139-E and was carried out while a Visitor at the Research School of Astronomy and Astrophysics (RSAA), Australian National University, supported by a RSAA visitors grant. M. Dopita acknowledges the support of the Australian National University and the Australian Research Council (ARC) through his ARC Australian Federation Fellowship, and also under ARC Discovery project DP0208445. The authors would like to thank Ernesto Oliva for his many helpful comments and for pointing out an error that the authors missed.

REFERENCES

Allen, M. G., Dopita, M. A., Tsvetanov, Z. I., & Sutherland, R. S. 1999, ApJ, 511, 686
Anders, E., & Grevesse, N. 1989, Geochim. Cosmochim. Acta, 53, 197
Baldwin, J. A., Ferland, G. J., Martin, P. G., Corbin, M. R., Cota, S. A., Peterson, B. M., & Slettebak, A. 1991, ApJ, 374, 580
Binette, L. 1998, MNRAS, 294, L47
Binette, L., Wilson, A. S., Raga, A., & Storchi-Bergmann, T. 1997, A&A, 327, 909
Binette, L., Wilson, A. S., & Storchi-Bergmann, T. 1996, A&A, 312, 365
Bottorff, M., Lamothe, J., Momjian, E., Verner, E., Vinković, D., & Ferland, G. 1998, PASP, 110, 1040
Cecil, G., Dopita, M. A., Groves, B., Ferruit, P., Pécontal, M., & Binette, L. 2002, ApJ, 568, 627
de Bruyn, A. G., & Wilson, A. S. 1978, A&A, 64, 433
Dopita, M. A. 2000, Ap&SS, 272, 79
Dopita, M.A., Heisler, C., Lumsden, S., & Bailey, J. 1998, ApJ, 498, 570
Dopita, M. A., & Sutherland, R. S. 1995, ApJ, 455, 468
———. 1996, ApJS, 102, 161
———. 2000, ApJ, 539, 742
Elitzur, M., & Ferland, G. J. 1986, ApJ, 305, 35
Ferguson, J. W., Korista, K. T., Baldwin, J. A., & Ferland, G. J. 1997, ApJ, 487, 122
Jones, A. P., Tielens, A. G. G. M., & Hollenbach, D. J. 1996, ApJ, 469, 740
Komossa, S., & Schulz, H. 1997, A&A, 323, 31
Kraemer, S. B., & Crenshaw, D. M. 2000, ApJ, 532, 256
Krolik, J. H., McKee, C., & Tarter, C. B. 1981, ApJ, 249, 422
Laor, A., & Draine, B. T. 1993, ApJ, 402, 441
Mathis, J. S., Rumpl, W., & Nordsieck, K. H. 1977, ApJ, 217, 425
Moorwood, A. F. M., Lutz, D., Oliva, E., Marconi, A., Netzer, H., Genzel, R., Sturm, E., & de Graauw, T. 1996, A&A, 315, L109
Netzer, H., & Laor, A. 1993, ApJ, 404, L51
Oliva, E., Salvati, M., Moorwood, A. F. M., & Marconi, A. 1994, A&A, 288, 457
Osterbrock, D. E. 1989, Astrophysics of Gaseous Nebulae and Active Galactic Nuclei (Mill Valley: University Science Books)
Pedlar, A., Meaburn, J., Axon, D. J., Unger, S. W., Whittle, D. M., Meurs, E. J. A., Guerrine, N., & Ward, M. J. 1989, MNRAS, 238, 863
Pier, E. A., & Voit, G. M. 1995, ApJ, 450, 628
Tadhunter, C. N., Robinson, A., & Morganti, R. 1989, in ESO Conf. Proc. 32, Workshop on Extranuclear Activity in Galaxies, ed. E. J. A. Meurs & R. A. E. Fosbury (Garching: ESO), 293
Tielens, A. G. G. M., McKee, C. F., Seab, C. G., & Hollenbach, D. J. 1994, ApJ, 431, 321
Veilleux, S. 1991a, ApJS, 75, 357
———. 1991b, ApJS, 75, 383
———. 1991c, ApJ, 369, 331
Veilleux, S., & Osterbrock, D. E. 1987, ApJS, 63, 295
Véron-Cetty, M. P., & Véron, P. 2000, A&A Rev., 10, 81
Wilson, A. S., & Raymond, J. C. 1999, ApJ, 513, L115
Wilson, A. S., & Willis, A. G 1980, ApJ, 240, 429